

## Rapid surface quality assessment of green 3D printed metal-binder parts

Kedarnath Rane<sup>\*a</sup>, Kevin Castelli<sup>b</sup>, Matteo Strano<sup>a</sup>

<sup>a</sup>*Dipartimento di Meccanica, Politecnico di Milano, Via La Masa 1, Milano, Italy*

<sup>b</sup>*Dipartimento di Ingegneria Meccanica e Industriale, Università degli Studi di Brescia, Via  
Branze 38, 25123, Brescia, Italy, k.castelli002@unibs.it*

*\*Corresponding author. Tel: +39-0223998534, E-mail: kedarnath.rane@polimi.it*

### Abstract

Mixtures made of a solid metal powder and a viscous polymeric binder are increasingly used in **material Extrusion Additive Manufacturing** (EAM) processes. The EAM process adopts the relative movement of an extruder head to a build table, to deposit thin strands of the mixture and build a 3D object layer by layer. In this study, EAM process was applied to produce 3D printed square plate-shaped parts of stainless steel 316L at the green state, i.e. before debinding and sintering. The 3D printing experiments were designed by considering various independent process parameters: extrusion velocity  $v_e$ , table velocity  $v_t$ , layer height  $h$  and hatch spacing  $D_a$ . The surface characteristics of as printed (green) square plate-shaped parts were investigated by a rapid, high-resolution optical imaging technique. The obtained images were analyzed to model the effect of the process parameters on the surface uniformity  $U_i$  and space filling  $F_i$ . The proposed methodology can be also used as a process monitoring technique. The study has demonstrated that the layer height  $h$  has the most relevant effect on the infill quality and should be set at a low value for good quality. However, a combination of the other parameters can be found that yields a compromise between infill surface quality and build up rate.

Keywords: *additive manufacturing; extrusion; feedstock; image processing; surface quality*

### 1. Introduction

In this paper, we use terminology a terminology according to the ISO/ASTM standard 52900, referring to additive manufacturing (AM) by material extrusion. The variants of material extrusion technologies are so numerous that the terminology itself might be confusing, so that some papers have been published focused on classification and terminology [1]. Many new material systems and combinations can today be extruded by AM, including short fiber reinforced thermoplastics [2,3]. The material Extrusion Additive Manufacturing (EAM) technique can also be used to deposit

a feedstock derived from the Metal Injection Molding (MIM) process, when the ultimate purpose is not to obtain a composite part but a full metal part. The typical MIM feedstock is made of metal fine powder, homogeneously mixed with a limited amount (usually less than 50% by volume) of a thermoplastic polymeric binder [4]. The extruded filament can be deposited according to a designed path, as in the Fused Deposition Modelling (FDM) techniques, for obtaining a 3D geometry [5]. The 3D printed feedstock is a so-called “green” part, still very soft, not yet capable of bearing any load except its own weight. In further steps of the process chain, thermal and solvent-based debinding techniques are used to remove water-soluble or organic binder constituents out of the green part. A porous “brown” structure is formed thereafter. The brown part is finally sintered to achieve desired densification and mechanical properties [6].

The EAM technique with green metal-polymer mixtures is rapidly growing, thanks to the recent availability of commercial equipment, but the scientific literature on this peculiar process is still very limited. In a recent review [7], the authors state that the idea of using highly-filled polymers for the additive manufacturing of metal parts was first introduced in the late 1990s and named fused deposition of metals (FDMet) [8]. It was based on the Stratasys FDM technology, in which highly-filled polymers with metal or ceramic particles are initially prepared as filaments, and then deposited according to the FDM principle.

An alternative type of feedstock has been recently proposed by some authors, made of pellets or granules produced as blends of polymeric binder and high solid powder loading [9]. Using high-pressure extruders was the technological innovation which enabled the use of highly dense and viscous thermoplastic-based feedstock, with viscosity values above 100 Pa·s. At the same time, the use of pellets or granules instead of filaments or pastes has allowed increasing the availability of material combinations and to use commercial powder injection molding materials. In 2010, a research group of Shenzhen University implemented an EAM process using a MIM feedstock [10]. They used a stainless-steel powder and thermoplastic paraffin wax-based binder, extruded through a screw extruder and they started studying the material properties of the green and sintered extruded filaments. Some years later, this idea was further developed at Politecnico di Milano [11], where a fully functional AM machine was built, combining a compact CNC controlled injection molding unit with a parallel kinematics (linear delta) table. This system can extrude a mixture with as much as 70% solid loading by volume. As demonstrated in [12], the mechanical properties of the deposited, debinded and sintered parts are comparable to the homogeneous wrought alloys. Very

recently, some commercial machines for the extrusion of metal-binder feedstock have been made available; the Desktop Metal Studio System has been proposed [13], based on the extrusion of a rod made of metal-binder mixture, rather than filaments or pellets.

### 1.1 Infill surface quality of 3Dprinted parts

The typical approach for building EAM parts is, for each layer to be deposited, to treat differently the outer contour profile (which mostly determines the outer surface quality of the parts) and the internal filling (infill) path (which mostly determines the mechanical strength). Sparse and fast filling techniques are used by most 3D printers for the internal infill roads, while the outer surface quality is controlled by reducing the speed of the contour profile and by using small layer heights, in order to reduce the staircase effect [14]. **In fact, for conventional FDM, a large amount of work has been done to correlate the many possible different infill strategies and parameters to the mechanical characterization of the 3D printed parts [15].** As a recent example, the paper [16] establishes the quantitative relationship between main parameters including layer thickness, infill rate, deposition velocity and tensile strength of FDM samples. However, the rheology, the cooling and solidification behavior of binders/polymers used in EAM of metals, which are highly loaded with metal powder, is different from the behavior of thermoplastic polymers used in conventional FDM. The available knowledge on conventional FDM cannot be automatically transferred to the EAM of metals. it is a frequent

Metal parts produced by EAM are meant to have mechanical applications, hence not only their outer appearance, outer surface quality and dimensional precision are relevant, but also their internal infill uniformity is relevant while depositing. In fact, the internal uniformity influences the final metallurgical homogeneity. To the authors' knowledge, no paper has been published that correlates the quality of horizontal infill surfaces, obtained by deposition paths of metal-polymer mixtures, to the process parameters. In [17], the nature and the origin of internal and external defects in the green deposited samples by FDMet is described systematically. The paper shows that the most serious defects were sub-perimeter voids and inter-road defects, that require process optimization to be reduced or suppressed. The paper suggests improving the internal quality by controlling the feedstock filament quality, by optimizing the build environment temperature and by using a negative gap between adjacent infill roads.

## 1.2 Optical assessment of surface quality through image processing

The purpose of the present paper is to determine a correlation between the main process parameters and the surface uniformity and quality of horizontal layers deposited by EAM of metals. The surface quality is assessed by taking binary images of the as-deposited (green) deposited layers.

While the quality of conventional FDM parts can be easily assessed with stylus-based devices, as in [18], in the present case, a contact system can damage the surface because the green parts are still very soft, not being sintered yet. Accordingly, measuring of the surface roughness with optical (non-contact) systems can eliminate these problems. The most accurate surface reconstruction with optical techniques could be performed with an optical 3D confocal microscope, as done in [19]. Alternatively, micro-ct scanning could be used to determine the internal micro-geometry of the samples, as in [20]. However, 3D optical reconstruction of surfaces, either by a confocal microscope or by a micro-ct scanner are a slow measurement processes that can require hours of scanning for a single specimen. Therefore, they are not suited for rapid process monitoring applications and, even less, could be applied in-situ. For this reason, 2d optical microscopic imaging has been used in the present study.

New methods are being developed in different fields to solve the problems of assessment of textures using machine vision programs of 2D images. In [21], the authors evaluated the statistical roughness parameters of image textures as spatial frequency and arithmetic average of grey levels, based on monochromatic speckle correlation. [22] assessed the surface roughness of machined parts by extracting features of surface roughness in the spatial frequency domain using the 2D Fourier transform. [23] developed a method of intensity distribution of binary image and an adaptive optics integrated system for measuring the surface roughness under dynamic turbulence. The application of dynamic speckle technology has been used by [24] for measuring surface roughness using image analysis of speckle pattern images. Artificial intelligence methods have also been frequently used, as in [25], where the MATLAB neural network toolbox has been used to assess the surface roughness of face milled steel samples.

In this study, a total of 48 experiments were conducted and one image for each experiment was taken using a digital microscope from the printed surfaces. A MATLAB routine has been developed to analyse thresholded binary images, with the aim of building a quantitative indicator of the filling degree of the deposited surfaces. In parallel, the aesthetical surface quality of the

samples has been assessed by showing the samples to a panel of 5 independent observers, averaging their scores.

## 2. Materials and methods

### 2.1 Feedstock preparation

A commercially available stainless steel powder (grade: SS316L; by Sandvik Osprey) having mean particle size  $8.8 \mu\text{m}$  (distribution:  $D_{10} = 4.1 \mu\text{m}$ ,  $D_{50} = 8.8 \mu\text{m}$ ,  $D_{90} = 15.9 \mu\text{m}$ ) was used as a raw material (Figure 1 (a)) for preparing feedstock. The chemical composition of powder is given in Table 1.

Table 1: Chemical composition of powder used in the present study

Element	Cr	Ni	Mo	Mn	Si	C	P	S	Fe
Wt.%	17.90	11.70	2.30	1.41	0.72	0.02	0.02	0.006	balance

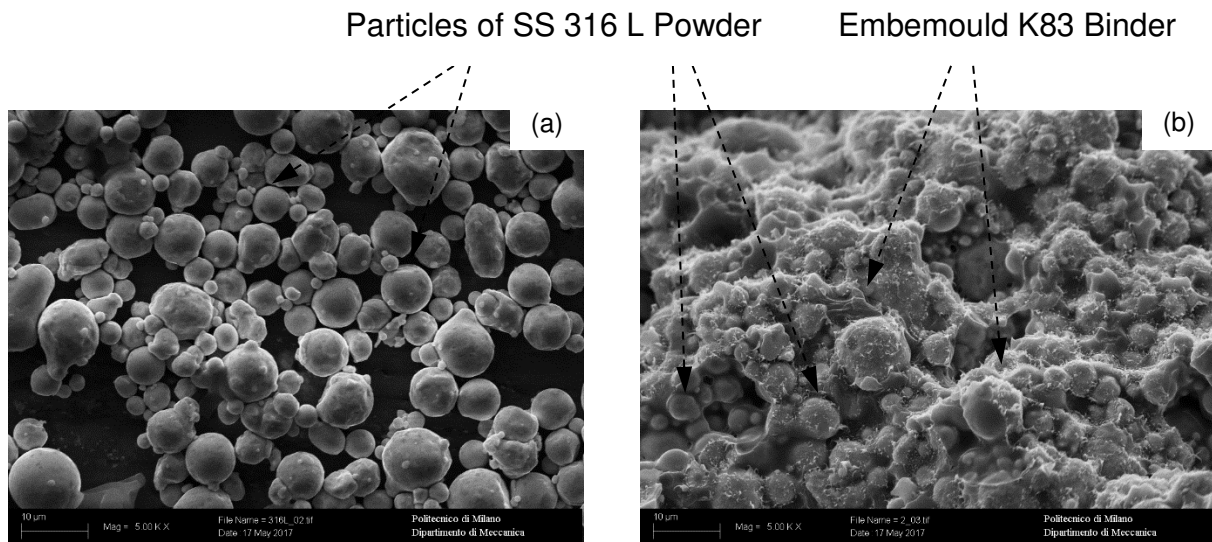


**Fig. 1.** SEM image of (a) SS316L powder and (b) fractured surface of feedstock pellet.

Commercial water-soluble binder (Embemould K83), a multi-component mixture (Density  $\rho = 1.05 \text{ g/cm}^3$ ), usually employed for powder injection moulding, was used to formulate the feedstock. Binder constituents and powder were premixed to obtain 92.5 wt. % powder loading in the feedstock using turbula mixer at room temperature. This mixture having about 63% by volume

powder loading was then compounded using a Brabender - Plasti-Corder mixer at 145°C for 30 minutes. This feedstock mixture was processed through a twin-screw extruder at 145°C to obtain a highly homogeneous (as appreciated from Figure 1 (b)) feedstock for subsequent operations.

## 2.2 3D printing experimental machine and setup

A specially designed and developed machine, called Ephæstus, shown in Figure 2 (a), was used for 3D printing tests. The machine is provided with a feedstock plasticizing and loader cylinder, heated and internally equipped with packed steel balls. The preheated melt flow enters the extrusion cylinder through a restricted gate. The pre-heating inside the feeding cylinder, the balls and the gate all provide shearing of the viscous flow and further homogenization of the feedstock. The temperature of feedstock inside the extrusion system was measured by means of three thermocouples: one at the feeding cylinder, one at the injection cylinder and one at the nozzle and was maintained constant at 110°C. The precise control of extrusion piston position and nozzle temperature ensures precise flow of molten feedstock. This machine is suitable for extruding varieties of feedstock mixture in required extrusion shapes, through a cylindrical exit nozzle (Figure 2 (b)). The synchronized movement of feeder piston supplies the molten feedstock to the extruder chamber and the extruder piston pushes the feedstock out of the nozzle for controlled extrusion and deposition.

The deposition is programmed according to a filling path, obtained by moving the robotic table placed under the extrusion unit. The deposition path is customised through a (g-code), which defines the coordinate-based trajectories for the outer perimeter and hatch (infill) of each layer, the extrusion velocity  $v_e$  and the table velocity  $v_t$ . Starting point of each layer is the same and not corresponding to the end point of the previous layer. In the present study, thin prismatic samples were 3D printed, with a square base of side length 40 mm. The samples are built depositing 4 layers of height  $h$ . **In conventional FDM, using infill patterns with a relative density smaller than 1 is a typical choice and the weight-to-strength ratio can be optimized with a proper infill pattern [26]. However, in this study we have selected a simple and common pattern strategy for the infill: each layer has two outer perimeters and the infill is printed with parallel rectilinear roads, alternating the direction of odd and even layers by 90, as shown in Figure 3 (a) and (b).**

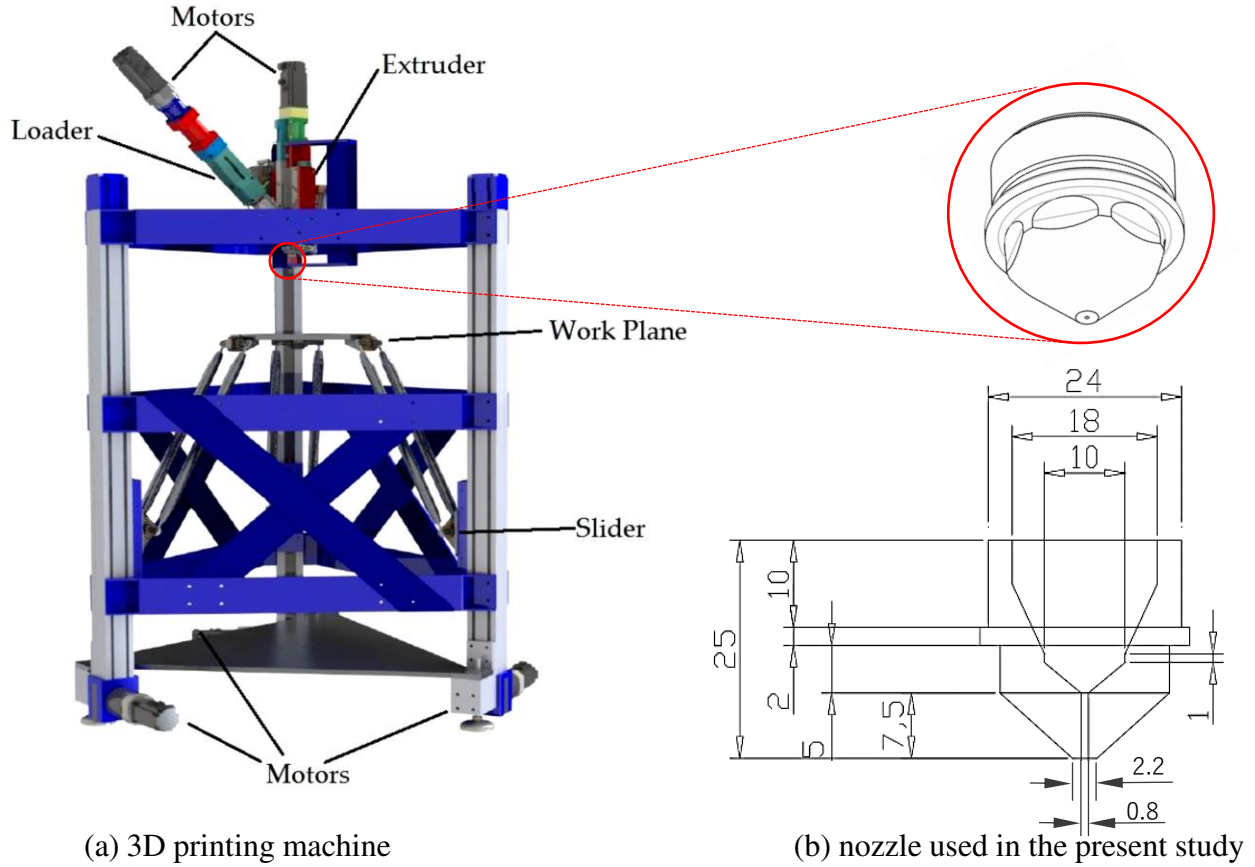


**Fig. 2.** Extrusion based additive manufacturing machine “Ephæstus”, with the dimensioned drawing of the extrusion nozzle.

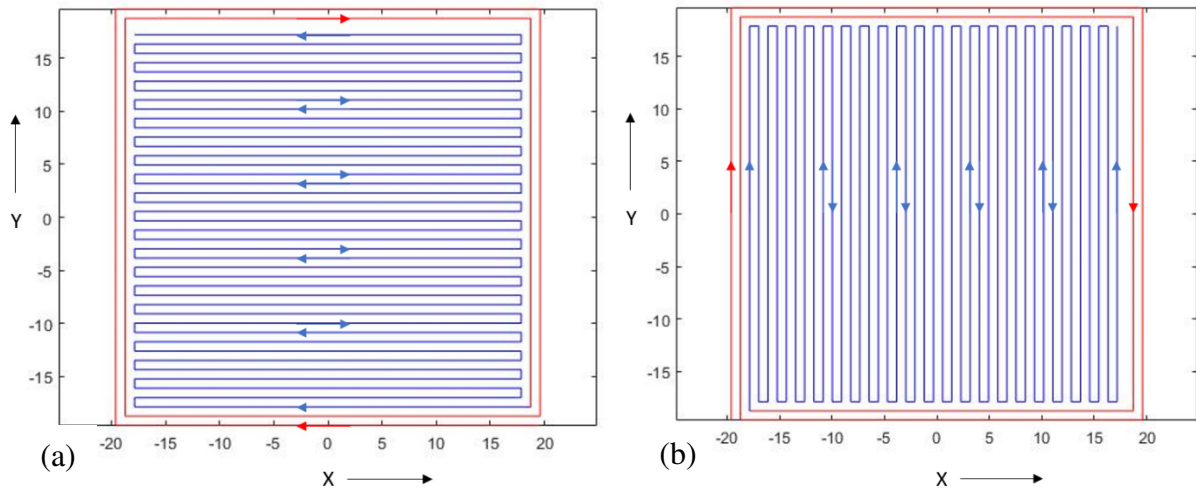


**Fig. 3.** A typical filling path with a two perimeters and unidirectional raster for (a) odd and (b) even layer of the part.

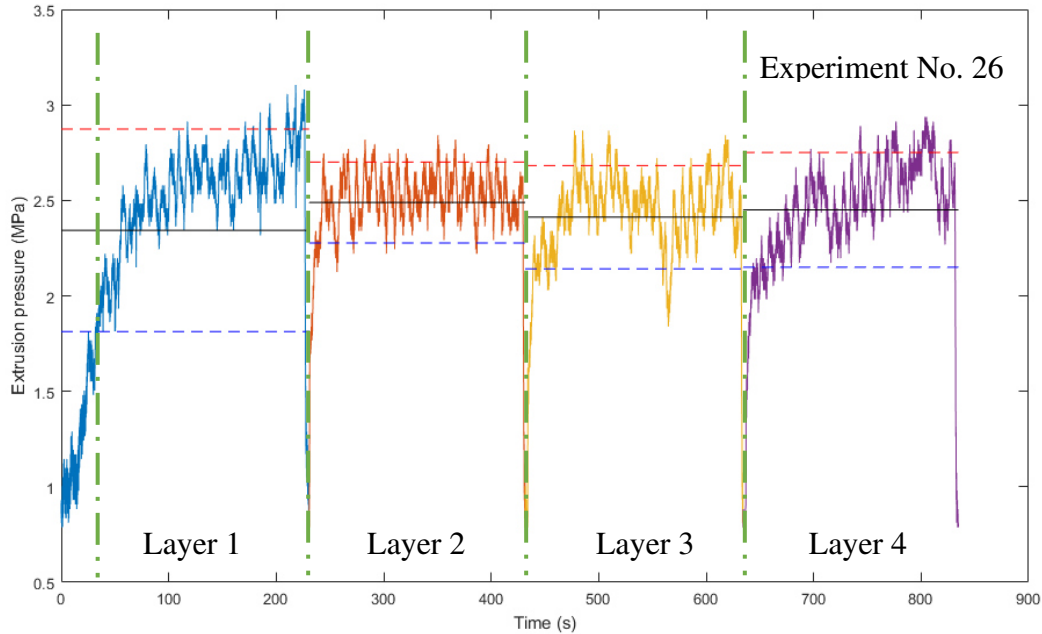


**Fig. 4.** Pressure vs. time signal recorded during one the experimental tests. During each layer, the pressure curve rapidly grows to a value and then stabilizes.

The extrusion unit is equipped with a vertical injection piston, which is numerically controlled. Out of each test, the electric power absorption of the drive of the CNC injection piston was recorded and converted into a pressure vs. time signal. An example of the pressure signal is shown in Figure 4. The pressure signal of the fourth layer, which is the upper and surface layer of each sample, has been analyzed: the central 5/7 portion of the signal has only been considered, the signal has been low pass filtered and the average extrusion pressure  $P_e$ , the standard deviation of the pressure  $\sigma_P$  and the noise-to-signal ratio  $\sigma_P/P_e$  have been calculated.

### 2.3 Selection of 3D printing parameters

One of the goals of the present study is to correlate the surface appearance and quality of the infill 3D printed green parts with the main control parameters of the extrusion based additive manufacturing (EAM) process of metal/binder feedstock. To obtain a full dense infill and a regular surface quality, a correct combination of process parameters must be identified. The main deposition parameters are:

- the hatch spacing  $D_a$ , which is the distance between two parallel adjacent roads in the infill tool path;

- the layer height  $h$ , which is the vertical distance between two layers scanned by the printing head;
- the extrusion nozzle diameter  $D_n$ ;
- the extrusion velocity  $v_e$  of the extruded filament at the nozzle exit;
- the velocity  $v_t$  of the deposition table.

If the extrusion velocity  $v_e$  and the nozzle diameter  $D_n$  are known, the extrusion flow rate is also known as:

$$Q = v_e \frac{\pi}{4} D_n^2 \dots\dots\dots (1)$$

The available knowledge for the selection of these parameters [27], which is also embedded in commercial software, has been developed for the conventional FDM machines and cannot be directly transferred to the EAM of metal/binder feedstock. Some assumptions and considerations must be made, when designing the process and the 3D printing experiments. The shape of the deposited road can be assumed as approximately rectangular, of height  $h$  and width  $w$ . According to the typical selected combinations of  $D_n$ ,  $h$  and  $v_e$  values, the actual resulting road width  $w$  is included within the range  $D_n \leq w \leq 2D_n$ . The obtained filling density of the green specimens (which in turn influences the final density of sintered specimens) depends primarily on the volumetric filling factor ( $\varphi$ ), defined as:

$$\varphi = \frac{v_t w h}{\psi Q} = 4 \frac{w h}{\psi \pi D_n^2} \frac{v_t}{v_e} \dots\dots\dots (2)$$

where  $\psi$  is the assumed swelling factor for EAM feedstock materials. The swelling factor is generally neglected in conventional extrusion models of FDM process. The pseudoplastic behavior of stainless steel 316L feedstock is likely to have viscoelastic (swelling) effects, i.e., partial recovery of the deformation that a viscoelastic fluid undergoes during the capillary flow of nozzle.

The condition for an ideal, perfect filling of the space during the deposition and for achieving a good surface uniformity is to obtain a road which is perfectly rectangular, with no empty spaces between adjacent roads and no overlaps. Hence the programmed distance between roads, i.e. the hatch spacing should be  $D_a = w$  and the fill factor should be selected as  $\varphi = 1$ . Under these assumptions, a full dense part and a regular surface can be obtained with:

$$D_a = w = \psi \frac{\pi D_n^2}{4h} \frac{v_e}{v_t} \dots\dots\dots (3)$$

However, the actual shape of the road is unknown, is not perfectly rectangular and it has rounded corners. Besides, the swelling factor  $\psi$  is also unknown. Thus, the selected  $D_a$  level might be wrong, i.e. different from the real  $w$ . This uncertainty is tested by assuming 4 possible values for  $\psi$  at 1, 1.05, 1.1 and 1.15, i.e. selecting the  $D_a$  value at the corresponding value. The highest  $\psi$ -value which yields full density and good surface quality will be considered the optimal swelling factor for the studied feedstock material. Technologically, higher  $\psi$ -values would be more convenient because the build-up rate ( $bur$ ) of the EAM process is equal to the product:

$$bur = v_t \cdot h \cdot D_a \dots\dots\dots (4)$$

and it is therefore directly proportional to  $\psi$ , according to equation (3).

As for the other parameters of equation (3), the following selections have been made. The nozzle diameter  $D_n$  has been kept fixed at 0.8 mm.

In conventional FDM, the  $h/D_n$  ratio must be  $< 1$  for a good deposition quality. Therefore, in the present study, this ratio has been varied over 3 levels: 0.7, 0.785, 0.87, by changing accordingly the  $h$  values. The infill density and the surface quality are also determined by the velocity of the extruded material  $v_e$  (which determines the shear rate and the viscosity of the melt) and has been varied at two levels (8 and 12 mm/s).

Finally, the ratio  $v_t/v_e$  has been varied at two levels (1.0 and 1.1) by changing the table velocity.

The resulting plan of experiments is made of 48 combinations: 2 levels of  $v_e$ , 2 levels of  $v_t/v_e$ , 3 levels of  $h$ , 4 assumed levels of  $\psi$  (i.e. 4 selected levels of  $D_a$ ).

### 2.3 Capturing and processing images for assessment of part characteristics

The 48 square plates were successfully printed using the Ephæstus machine shown in Figure 3, according to the plan of experiments defined in Section 2.2. Some representative green and sintered parts are shown in Figure 4. The dimensional accuracy of the printed parts is in the limits allowed by the positioning precision of the deposition table. The dimensions of sintered parts (Figure 5 (b)) are smaller than green parts (Figure 5 (a)), because of shrinkage after sintering, with the side of the square sample that shrinks of about.

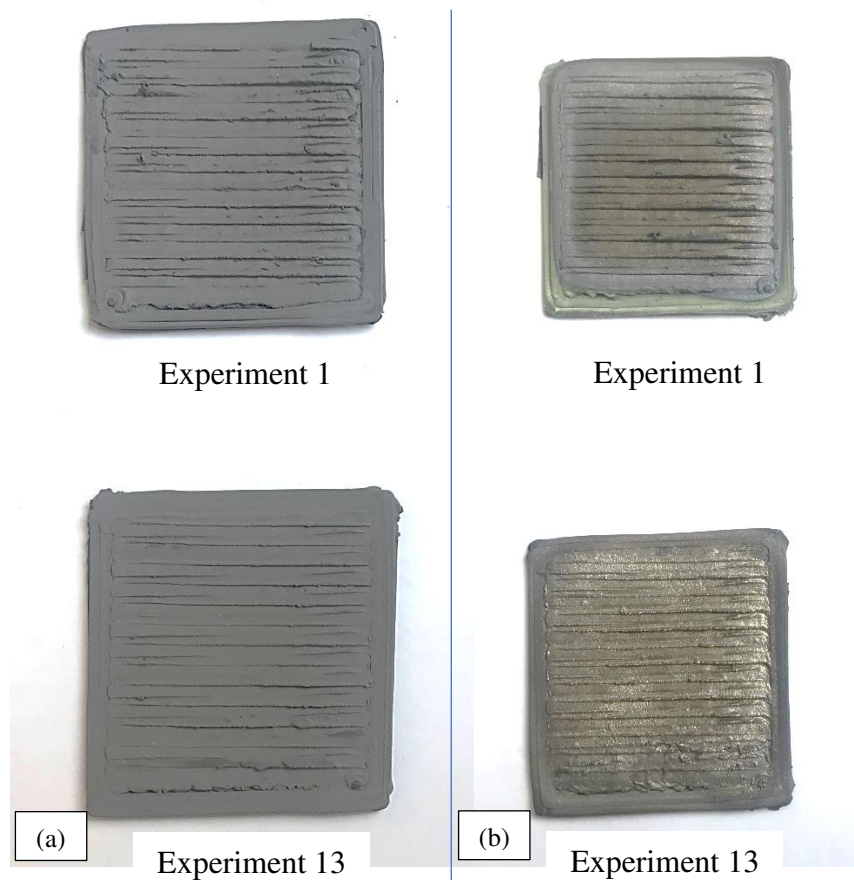


**Fig. 5.** Square plate shaped parts: (a) after 3D printing and (b) after sintering

After 3D printing tests, images of the top infill surface were taken using an optical digital stereo microscope (SM 353 H by EchoLAB) with a magnification factor of 65. The obtained images from the surfaces were processed in MATLAB®, according to the method described as follows.

First, greyscale images were adjusted for brightness and contrast, using the command *imadjust* of the MATLAB® image processing toolbox. The images were then converted into binary format, pixels in binary images with a value of 0, were displayed as black, and pixels with the value of 1 were displayed as white. The binary conversion of image generates a two dimensional matrix with 3981312 pixels data having units of 0 and 1. In Figure 6 (b), the black areas on the binary image represent depressions of the sample surface, mostly visible at the interface between adjacent roads. The white areas define the higher levels of the road width, where the road has been properly filled. The linear tracks in the Y direction in the image are aligned with the road orientation during the EAM process. On each image, the profiles of 15 lines crossing the sample in the X direction were

generated, perpendicular to the road direction. The profiles are a sequence of black (empty) and white (filled) segments. Each profile undergoes a filtering process, deleting all segments with a length smaller than 10 pixels. An example of binary profile resulting after the filtering process is shown in Fig. 5(c). Finally, the segments are converted from pixel to length (pixels/mm: 5/592).

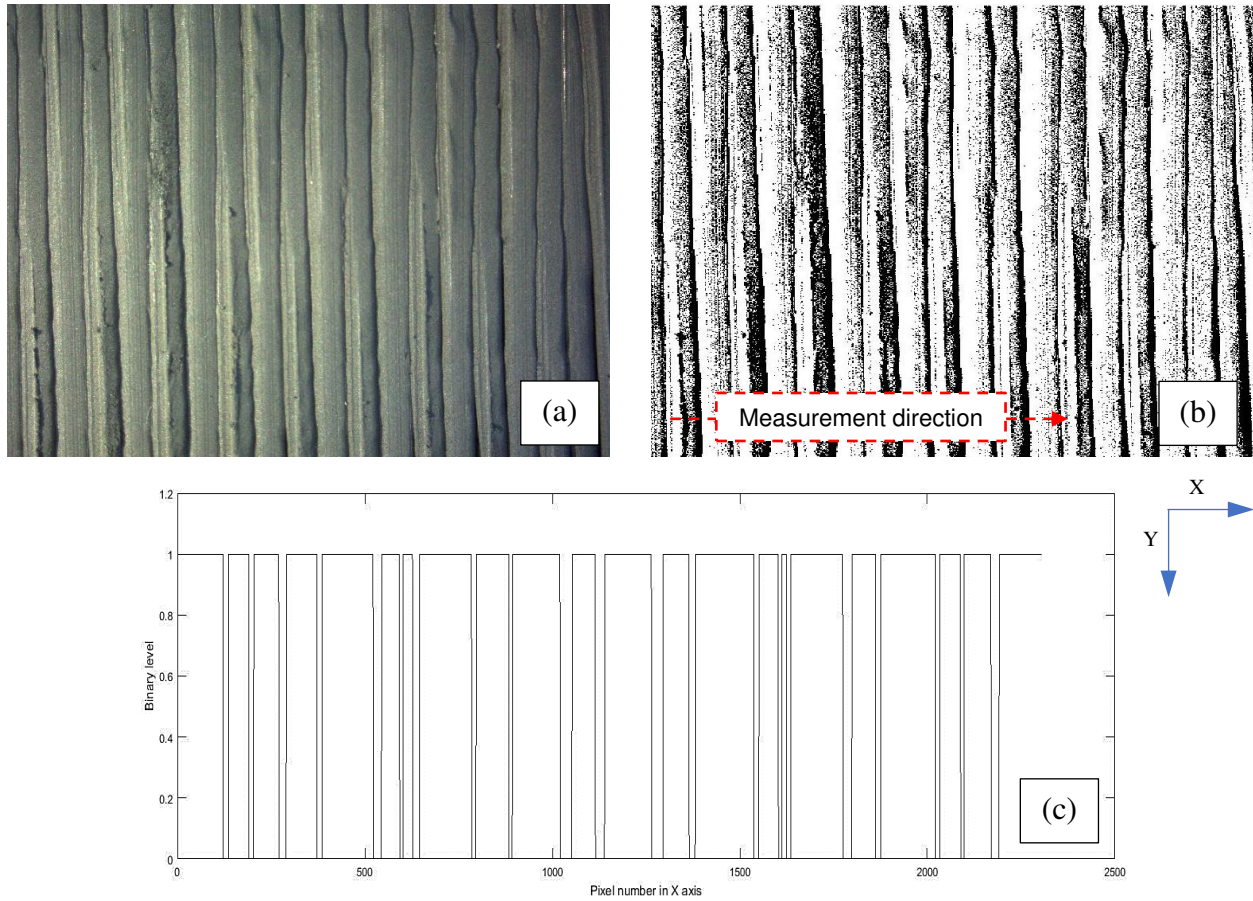


**Fig. 6.** Applied order for image analysis (a) capturing image using optical microscope, (b) converting to binary image, (c) period identification.

Each white segment  $i$ , belonging to each profile  $j$ , on the surface of each sample  $k$  has a length  $l_{ijk}$  in the X direction. This length can be compared with the printing parameter, especially  $D_a$  and  $OD_n$ . Four cases can be identified:

- Case 1 : If  $l_{ijk} < D_a$ , the combination of the printing parameters generates underfilling and, therefore, surface depressions and irregularities. For each sample  $k$ , the total number of segments that can be classified under Case 1 is recorded in the variable  $n_1$ .
- Case 2 : When  $l_{ijk} \approx D_a$ , the volume of the extruded road material completely occupies the available space created by combination of printing parameters. For each sample  $k$ , the total number of segments that can be classified under Case 2 is recorded in the variable  $n_2$ .
- Case 3 : When  $D_a < l_{ijk} < OD_n$ , the combination of the printing parameters generates overfilling, i.e. the road width is greater than the hatch spacing. The number of segments classified under Case 3 is recorded in the variable  $n_3$ .
- Case 4 : When  $D_a < l_{ijk} \approx OD_n$ , the combination of the printing parameters generates overfilling and the excess material builds up and interacts with the outer diameter of nozzle ( $OD_n = 2.2$  mm, shown in Fig. 2). The number of segments classified under Case 4 is recorded in the variable  $n_4$ .

The number of segments belonging to each classification, from  $n_1$  to  $n_4$  have been used to build a global indicator of surface uniformity (quality) and filling and can be used for process control and other purposes. Cases 1 and 4 can be considered pathologic, while it would be preferable that most segments fall within cases 2 and 3. Two main indicators of quality have been developed: a uniformity index  $Ui$  and a filling index  $Fi$ , defined as follows:

$$Ui = \frac{1/3n_2 + 2/3n_3}{n_1 + n_2 + n_3 + n_4}; Fi = \frac{1/3n_3 + 2/3n_4 - n_1}{n_1 + n_2 + n_3 + n_4} \dots\dots\dots (5)$$

$Ui$  is a measure of uniformity of the surface, because it gives larger values when most segments fall within categories 2 and 3, i.e. when their length is equal to or slightly larger than the programmed hatch spacing  $D_a$ .

$Fi$  is a filling indicator, because it positively counts the number of segments that are longer than  $D_a$  ( $n_3$  and  $n_4$ ) and subtracts the number of segments that indicate under filling ( $n_1$ ).

While  $Fi$  and  $Ui$  are objective experimental measurement of the surface quality of the green samples, they do not provide an obvious indication of cosmetic quality, which is subjective, and difficult to be expressed by a numerical measurement out of the 2D microscopic images. For this reason, a panel of 5 independent researchers have been shown the images and asked to assign them

a cosmetic quality value, in a range from 1 to 3, where 1 indicates a poor quality and 3 a good quality. The average of the five quality values has been taken as a global indicator  $Q_i$  of aesthetical quality of each sample.

### 3. Results and discussion

#### 3.1 Extrusion pressure variation with extrusion velocity

The measured experimental pressure values  $P_e$  and  $\sigma_P/P_e$  depend on the extrusion parameters, namely the extrusion velocity  $v_e$ , the extrusion temperature and the nozzle diameter  $d_n$ . In the considered plan of experiments, only the velocity  $v_e$  has been changed. The dependence of the pressure average and variations on the extrusion velocity are shown in Figure 7. Since the data in fig. 7 evidence a large natural variability of the pressure signal, which increases with the extrusion velocity, there is a potential influence of the pressure fluctuations onto the surface characteristics of the samples, as measured by the filling  $Fi$ , uniformity  $Ui$  and cosmetic quality  $Qi$  indicators. However, a statistical analysis of the results of the experiments has shown that there is no clear and direct correlation between the surface responses ( $Fi$ ,  $Qi$  and  $Ui$ ) and the pressure values ( $P_e - \sigma_P/P_e$ ) of each test. In other words, the infill surface quality of the deposited green samples is not influenced by the variability of the pressure conditions.

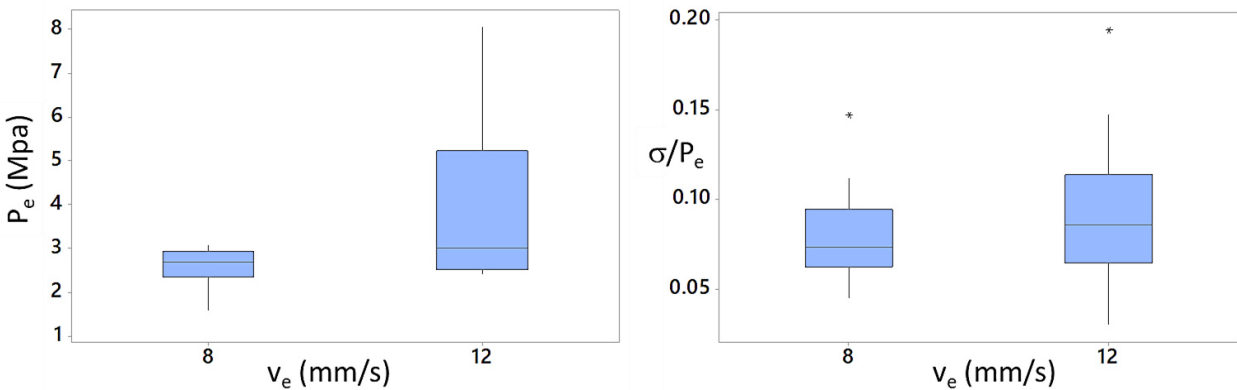


**Fig. 7.** Boxplots of the measured average extrusion pressure  $P_e$  and noise-to-signal  $\sigma_P/P_e$ .

### 3.2 Effect of deposition parameters on filling and uniformity indicators

The measured surface characteristics of the green 3D printed samples are influenced by the process parameters. A statistical analysis of the 48 available experimental results has been performed using the filling  $Fi$  and uniformity  $Ui$  as response variables. Linear regression models have been built, performing F-tests on the statistical significance of the regressor terms.

The results clearly indicate that  $Fi$  depends on the combination of  $v_e$ ,  $v_t/v_e$  and  $h$ . A graphical representation of this dependence is given in Figure 8. Higher filling can be obtained with lower extrusion speed  $v_e$ , lower table transverse velocity  $v_t/v_e$  and lower layer height  $h$ . Surprisingly, the filling factor does not depend on the assumed  $\psi$  level. Physically, this means that in the investigated range (1 to 1.15), the selection of the factor  $\psi$  and therefore the selection of  $D_a$ , according to equation (3), does not significantly influence the apparent surface filling. Since the build-up rate  $bur$  is the product of  $v_t \cdot h \cdot D_a$ , the hatch spacing can be safely and conveniently selected at the maximum level, obtained when  $\psi=1.15$ . On the contrary,  $h$  and  $v_t/v_e$  must be kept at a low level, if higher filling is of interest.

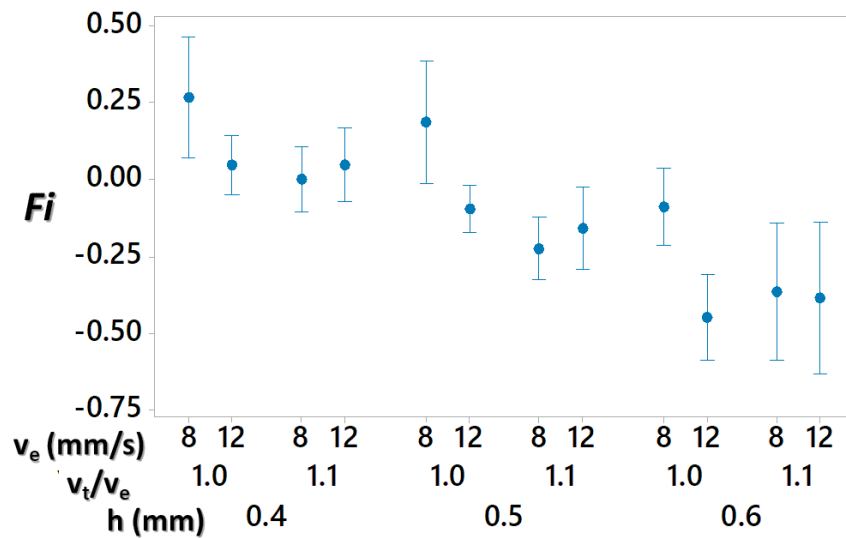


**Fig. 8.** A 95% confidence interval plot of the measured filling indicator  $Fi$  vs the significant deposition parameters.

The results of the statistical analysis indicate that the uniformity indicator  $Ui$  mostly depends on the selected  $h$  level, i.e. it significantly improves when the layer height is smaller. Besides, there is a mild influence of  $v_e$  and  $\psi$ , i.e. the uniformity slightly improves with larger extrusion speed

and larger  $\psi$ -value. A graphical representation of the dependence of  $U_i$  on  $h$  and  $v_e$  is given in Figure 9.

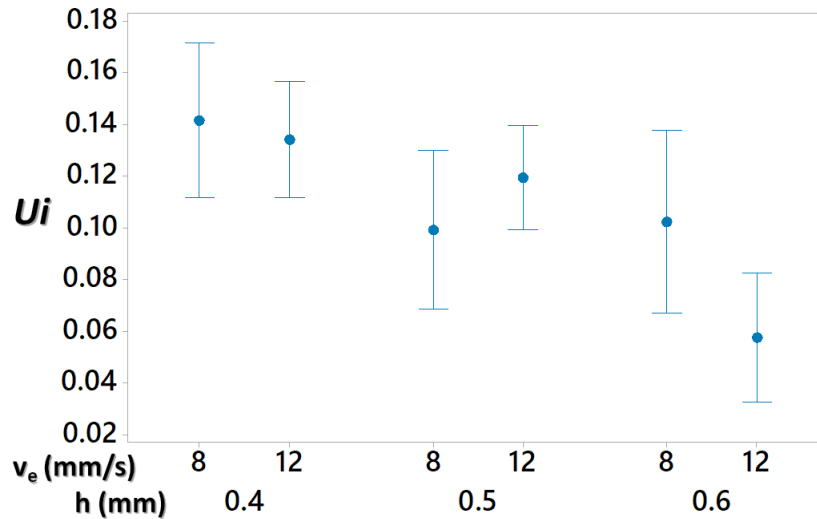


**Fig. 9.** A 95% confidence interval plot of the measured uniformity indicator  $U_i$  vs.  $h$  and  $v_e$ .

In conclusion, the results indicate that the surface quality of the infill of green 3D printed parts is mostly influenced by the layer height  $h$ , which should be as small as possible. Besides, the filling and the uniformity improve when the extrusion speed  $v_e$  and the table speed  $v_t$  are low, i.e. for a slow process. Finally, the surface quality is not significantly influenced (in the investigated range) by the hatch spacing, which can be selected at a high level, with a positive effect on the build-up rate and on the surface uniformity.

### 3.3 Effect of deposition parameters on cosmetic surface quality

The indicator  $Q_i$  of aesthetical surface quality is also influenced by the process parameters. It must be observed that the subjective perception of surface quality  $Q_i$ , as quantified by 5 independent observers, is surprisingly not correlated with the objective indicators of filling and uniformity  $F_i$  and  $U_i$ . In fact, while  $F_i$  and  $U_i$  substantially do not depend on the swelling factor  $\psi$ , this is not the case for  $Q_i$ . It appears that (from Figure 10) the best surface appearance of the top layer is obtained when the layer height  $h$  is small (0.4 mm) and  $\psi = 1.05$  to 1.10.

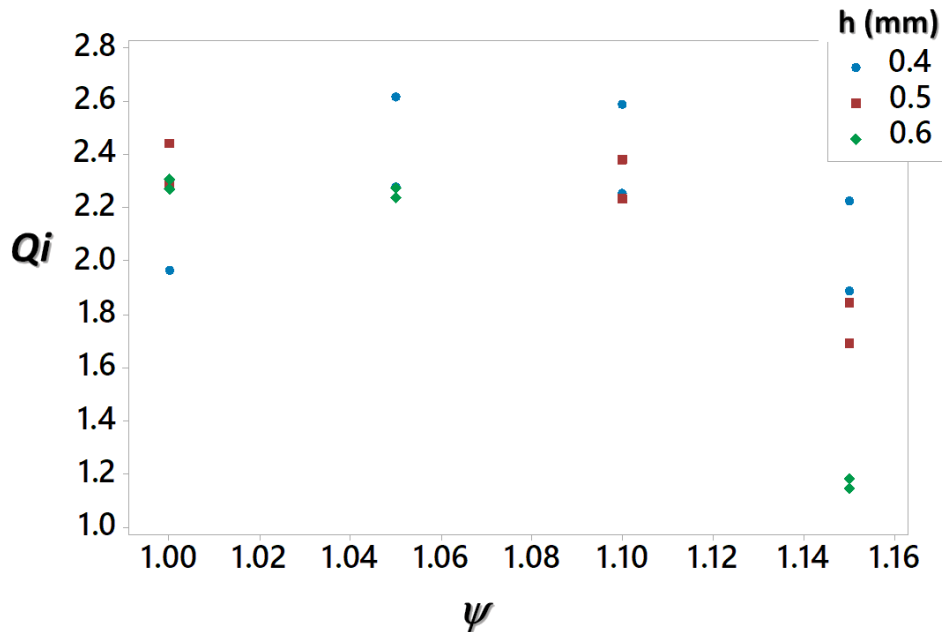


**Fig. 10.** Fitted values of a regression model on  $Q_i$  vs. the process parameters, including a quadratic term on the  $\psi$  factor.

### 3.4 Discussion of results

A good infill surface quality of EAM green parts (made of a mixture of metal powder and polymeric binder) favors adhesion of the layers while 3D printing and positively influences the metallurgical quality of the final sintered parts. However, it would be useful to obtain an acceptable surface quality with large build-up rate  $bur$  (the product of  $v_r \cdot h \cdot D_a$ ), to improve productivity. In the investigated range, the  $bur$  was varied from a minimum of  $0.23 \text{ cm}^3/\text{min}$  to a maximum of  $0.44 \text{ cm}^3/\text{min}$ . The results presented in Sections 3.2 and 3.3 clearly show that the quality of the infill surface of sintered parts is significantly influenced by the layer height  $h$ . The three developed indicators of filling, uniformity and aesthetical quality all increase when the smallest tested  $h$ -value (0.4 mm) is used, which is half of the nozzle diameter  $d_n$  (0.8 mm). All other parameters have a minor influence, and they can be selected in order to increase the  $bur$ , i.e. the productivity of the process. When  $h=0.4 \text{ mm}$ , increasing the extrusion velocity  $v_e$  at 12 mm/s, the table velocity ratio  $v_r/v_e$  at 1.1 and the  $\psi$ -value at 1.1, there is no detrimental effect on uniformity and on cosmetic quality (see Figures 9 and 10); the corresponding productivity is  $bur= 0.35 \text{ cm}^3/\text{min}$ .

## 4. Conclusions

In this paper, a method has been developed for processing of 2D microscopic images taken on the infill horizontal surfaces of 3D printed sample, obtained by extrusion of a mixture of metal powder and polymeric binder. Two quantitative indicators of surface uniformity  $U_i$  and space filling  $F_i$  have been extracted by the image processing routine. The method has been used in the paper for correlating the infill surface quality to the 3D printing process parameters. Besides, the proposed method can be used, in the future, for process monitoring and quality control purposes. Furthermore, a cosmetic quality indicator has also been used to estimate the perceived quality of the green samples. The results indicate that the most relevant process parameter on the surface quality is the layer height, which should be kept at a low value. The influence of extrusion speed, table speed and hatch spacing is less significant, therefore a compromise on the other parameters can be found, so that the build-up rate of the 3D printing process can be set at a medium-high level (referring to the investigated range of experimental parameters), with no detrimental effects on surface quality.

## Acknowledgments

The authors wish to thank Mr. Valerio Mussi of the MUSP research lab ([www.musp.it](http://www.musp.it)) of Piacenza (Italy), for his precious help in the debinding and sintering operations.

## References

- [1] Lee JM, Sing SL, Zhou M, Yeong WY. 3D bioprinting processes: A perspective on classification and terminology. *Int J Bioprinting* 2018;4. doi:10.18063/ijb.v4i2.151.
- [2] Bedi P, Singh R, Ahuja I. Effect of SiC/Al<sub>2</sub>O<sub>3</sub> particle size reinforcement in recycled LDPE matrix on mechanical properties of FDM feed stock filament. *Virtual Phys Prototyp* 2018;13:246–54. doi:10.1080/17452759.2018.1496605.
- [3] Goh GD, Dikshit V, Nagalingam AP, Goh GL, Agarwala S, Sing SL, et al. Characterization of mechanical properties and fracture mode of additively manufactured carbon fiber and glass fiber reinforced thermoplastics. *Mater Des* 2018;137:79–89. doi:10.1016/j.matdes.2017.10.021.
- [4] Kong X, Barriere T, Gelin JC. Determination of critical and optimal powder loadings for 316L fine stainless steel feedstocks for micro-powder injection molding. *J Mater Process Technol* 2012;212:2173–82. doi:10.1016/j.jmatprotec.2012.05.023.
- [5] Masood S., Song W. Development of new metal/polymer materials for rapid tooling using Fused deposition modelling. *Mater Des* 2004;25:587–94. doi:10.1016/j.matdes.2004.02.009.

- [6] Páez-Pavón A, Jiménez-Morales A, Rodríguez-Arbaizar M, Carreño-Morelli E, Torralba JM. Sintering optimisation of Fe–Si soft magnetic materials processed by metal injection moulding. *Powder Metall* 2017;60. doi:10.1080/00325899.2017.1289631.
- [7] Gonzalez-Gutierrez J, Cano S, Schuschnigg S, Kukla C, Sapkota J, Holzer C. Additive Manufacturing of Metallic and Ceramic Components by the Material Extrusion of Highly-Filled Polymers: A Review and Future Perspectives. *Materials (Basel)* 2018;11:840. doi:10.3390/ma11050840.
- [8] Wu G, A. Langrana N, Sadanji R, Danforth S. Solid freeform fabrication of metal components using fused deposition of metals. *Mater Des* 2002;23:97–105. doi:10.1016/S0261-3069(01)00079-6.
- [9] Rane K, Cataldo S, Parenti P, Sbaglia L, Mussi V, Annoni M, et al. Rapid production of hollow SS316 profiles by extrusion based additive manufacturing. *AIP Conf. Proc.*, vol. 1960, 2018. doi:10.1063/1.5035006.
- [10] Li J Bin, Xie ZG, Zhang XH, Zeng QG, Liu HJ. Study of Metal Powder Extrusion and Accumulating Rapid Prototyping. *Key Eng Mater* 2010;443:81–6. doi:10.4028/www.scientific.net/KEM.443.81.
- [11] Annoni M, Giberti H, Strano M. Feasibility Study of an Extrusion-based Direct Metal Additive Manufacturing Technique. *Procedia Manuf* 2016;5:916–27. doi:10.1016/j.promfg.2016.08.079.
- [12] Ren L, Zhou X, Song Z, Zhao C, Liu Q, Xue J, et al. Process Parameter Optimization of Extrusion-Based 3D Metal Printing Utilizing PW–LDPE–SA Binder System. *Materials (Basel)* 2017;10:305. doi:10.3390/ma10030305.
- [13] Bose A, Schuh CA, Tobia JC, Tuncer N, Mykulowycz NM, Preston A, et al. Traditional and additive manufacturing of a new Tungsten heavy alloy alternative. *Int J Refract Met Hard Mater* 2018;73:22–8. doi:10.1016/j.ijrmhm.2018.01.019.
- [14] Boschetto A, Bottini L. Accuracy prediction in fused deposition modeling. *Int J Adv Manuf Technol* 2014;73:913–28. doi:10.1007/s00170-014-5886-4.
- [15] Srivastava M, Rathee S. Optimisation of FDM process parameters by Taguchi method for imparting customised properties to components. *Virtual Phys Prototyp* 2018;13:203–10. doi:10.1080/17452759.2018.1440722.
- [16] Li H, Wang T, Sun J, Yu Z. The effect of process parameters in fused deposition modelling on bonding degree and mechanical properties. *Rapid Prototyp J* 2018;24:80–92. doi:10.1108/RPJ-06-2016-0090.
- [17] Agarwala MK, Jamalabad VR, Langrana N a, Safari A, Whalen PJ, Danforth SC. Structural quality of parts processed by fused deposition. *Rapid Prototyp J* 1996;2:4–19. doi:10.1108/13552549610732034.
- [18] Nuñez PJ, Rivas A, García-Plaza E, Beamud E, Sanz-Lobera A. Dimensional and Surface Texture Characterization in Fused Deposition Modelling (FDM) with ABS plus. *Procedia Eng* 2015;132:856–63. doi:10.1016/j.proeng.2015.12.570.
- [19] Lee JM, Zhang M, Yeong WY. Characterization and evaluation of 3D printed microfluidic chip for cell processing. *Microfluid Nanofluidics* 2016;20:5. doi:10.1007/s10404-015-

1688-8.

- [20] Quan Z, Suhr J, Yu J, Qin X, Cotton C, Mirotznik M, et al. Printing direction dependence of mechanical behavior of additively manufactured 3D preforms and composites. *Compos Struct* 2018;184:917–23. doi:10.1016/j.compstruct.2017.10.055.
- [21] Dhanasekar B, Mohan NK, Bhaduri B RB. Evaluation of surface roughness based on monochromatic speckle correlation using image processing. *Precis Eng Eng* 2008;32:196–206.
- [22] Tsai D-M, Chen J-J, Chen J-F. A vision system for surface roughness assessment using neural networks. *Int J Adv Manuf Technol* 1998;14:412–22. doi:10.1007/BF01304620.
- [23] Fuh Y-K, Hsu KC, Fan JR. Roughness measurement of metals using a modified binary speckle image and adaptive optics. *Opt Lasers Eng* 2012;50:312–6. doi:10.1016/j.optlaseng.2011.11.003.
- [24] Kayahan E, Oktem H, Hacizade F, Nasibov H, Gundogdu O. Measurement of surface roughness of metals using binary speckle image analysis. *Tribol Int* 2010;43:307–11. doi:10.1016/j.triboint.2009.06.010.
- [25] Samtaş G. Measurement and evaluation of surface roughness based on optic system using image processing and artificial neural network. *Int J Adv Manuf Technol* 2014;73:353–64. doi:10.1007/s00170-014-5828-1.
- [26] Zhou X, Hsieh SJ, Ting CC. Modelling and estimation of tensile behaviour of polylactic acid parts manufactured by fused deposition modelling using finite element analysis and knowledge-based library. *Virtual Phys Prototyp* 2018;13:177–90. doi:10.1080/17452759.2018.1442681.
- [27] Anitha R, Arunachalam S, Radhakrishnan P. Critical parameters influencing the quality of prototypes in fused deposition modelling. *J Mater Process Technol* 2001;118:385–8. doi:10.1016/S0924-0136(01)00980-3.